Graphene Coatings: Probing the Limits of the One Atom Thick Protection Layer

Louis Nilsson, Mie Andersen, Richard Balog, Erik Lægsgaard, Philip Hofmann, Flemming Besenbacher, Bjørk Hammer, Ivan Stensgaard, and Liv Hornekær*

Department of Physics and Astronomy and Interdisciplinary Nanoscience Center iNANO, Aarhus University, DK-8000 Aarhus C, Denmark

ABSTRACT The limitations of graphene as an effective corrosion-inhibiting coating on metal surfaces, here exemplified by the hex-reconstructed Pt(100) surface, are probed by scanning tunneling microscopy measurements and density functional theory calculations. While exposure of small molecules directly onto the Pt(100) surface will lift the reconstruction, a single graphene layer is observed to act as an effective coating, protecting the reactive surface from O_2 exposure and thus preserving the reconstruction underneath the graphene layer in O_2 pressures as high as 10^{-4} mbar. A similar protective effect against CO is observed at CO pressures below 10^{-6} mbar. However, at higher pressures CO is observed to intercalate under the graphene coating layer, thus lifting the reconstruction. The limitations of the coating effect are further tested by exposure to hot atomic hydrogen. While the coating can withstand these extreme conditions for a limited amount of time, after substantial exposure, the Pt(100) reconstruction is lifted. Annealing experiments and density functional theory calculations demonstrate that the basal plane of the graphene stays intact and point to a graphene-mediated mechanism for the H-induced lifting of the reconstruction.

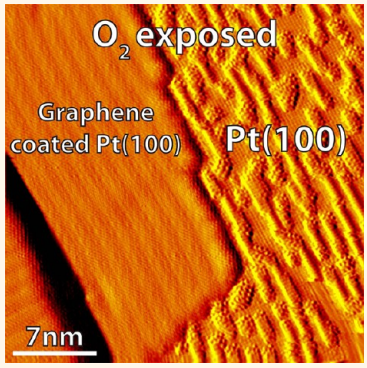

KEYWORDS: graphene · coating · STM · hydrogen · CO · O_2

Graphene, a single layer of carbon atoms,[1] combines several exceptional properties, which makes it uniquely suited as a coating material: excellent mechanical stability, low chemical reactivity, impermeability to most gases, transparency, flexibility, and very high thermal and electrical conductivity.[2] Moreover, graphene can be grown directly on a range of metal surfaces and is even able to cover step edges and small defects in metal surfaces in a carpet-like fashion.[3−5] As a result, research into graphene as a coating material is now rapidly intensifying.[6−16] Building on the long-time experience with graphene films on metal surfaces[17] and the coking effect of carbon layers on metal catalysts,[18] investigations are now focusing on the limitations of graphene coatings caused by defects and domain boundaries in the graphene.[6,9,11,12,16] Graphene coatings have been observed to reduce the electrochemical corrosion rate of nickel and copper[11,12] and to protect copper and copper/nickel alloys from air oxidation under ambient conditions.[9] However, O_2 was observed to intercalate under graphene coatings on Ru(0001) at elevated temperatures,[6] and CO was observed to intercalate under graphene on Pt(111) at room temperature.[16] Less attention has been paid to the coating limitations of the basal plane of graphene, with the exception of a recent theoretical article investigating the protection of Al(111) from oxidation by a graphene coating.[10]

Here we use scanning tunneling microscopy (STM) to investigate the effectiveness of a graphene coating on the reactive, hex-reconstructed Pt(100) surface toward CO and O_2 at a wide range of partial pressures. Moreover, we test the limitations of the graphene coating on Pt(100) by exposing it to hot atomic hydrogen and investigate the resulting structures with STM measurements, temperature-programmed desorption (TPD) spectroscopy, and density functional theory (DFT) calculations. The Pt(100) surface was chosen as substrate, because the reconstruction of the surface is lifted if the surface reacts with, for example, CO, O_2, or H atoms.[19,20] Furthermore, the reconstruction of the Pt(100) surface is still present under

* Address correspondence to liv@phys.au.dk.

Received for review September 3, 2012 and accepted October 29, 2012.

Published online October 29, 2012
10.1021/nn3040588

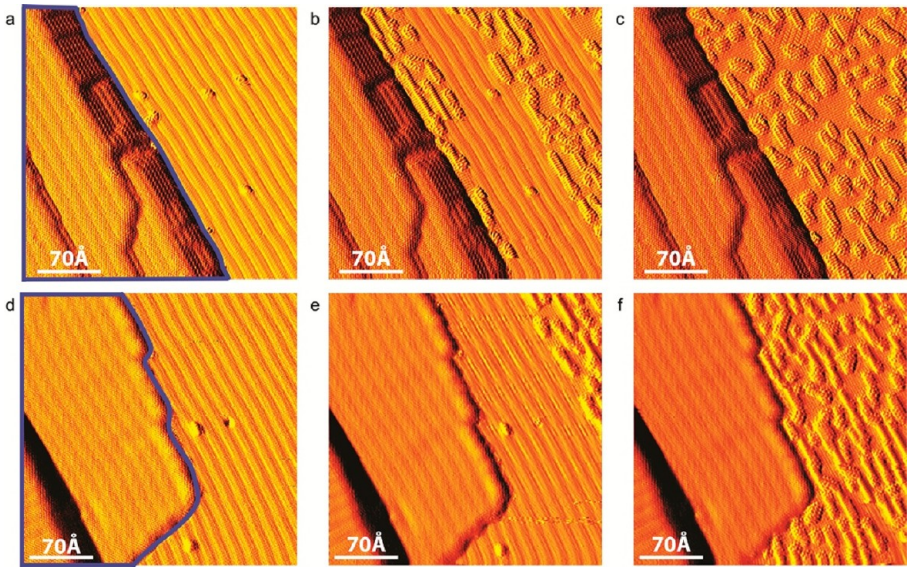

Figure 1. STM image of a Pt(100) surface partially coated by graphene. For all images, the terrace at the right side is uncoated, whereas the rest is coated by graphene (indicated by a blue boundary). (a–c) Partially coated surface exposed to 0, 3, and 63 L of CO, respectively. (d–f) Partially coated surface exposed to 0, 25, and 40 L of O_2, respectively. All the images have been differentiated to enhance the contrast. Imaging conditions [Vt, It]: (a–c) [4.6 mV, 0.44 nA]; (d–f) [4.3 mV, 0.48 nA].

the graphene coating and can be depicted (through the graphene) by STM.[5] The presence of the reconstruction can therefore be used as an indicator to determine if the coating is effective toward various gases.

RESULTS AND DISCUSSION

An STM image of a Pt(100) surface partially coated with graphene is displayed in Figure 1a. The upper right terrace is the clean reconstructed Pt(100) surface, whereas the lower left terraces are covered with graphene. The fact that the graphene sheet is formed continuously over the step edges[5] results in a nearly perfect coating without any defects, whereas a few defects are observed at the uncoated terrace. By *in situ* exposure of the partially graphene-coated Pt(100) surface, held at room temperature, to CO while imaging the surface by STM, the real-time development can be followed. The same area imaged after 3 L of CO and 63 L of CO is shown in Figure 1b and c, respectively. It is seen that the reconstructed Pt(100) surface gradually reacts with the CO molecules, which induces a lifting of the reconstruction, visible by the formation of bright irregular islands. However, no change is observed on the graphene-coated Pt(100) terraces, even after exposures as high as 500 L and at gas pressures as high as 3×10^{-7} mbar. Even at the edge of the graphene sheet, toward the unprotected area of Pt(100), the coating withstands the exposure of CO and the reconstruction of the Pt(100) surface is undisturbed under the graphene coating. From these findings we deduce that graphene is a very efficient coating toward CO at these partial pressures.

Similar experiments were performed by exposing a partially graphene-coated Pt(100) surface held at room temperature to O_2 molecules. The results are shown in Figure 1d to f. Figure 1d shows the unexposed surface, in which the right terrace is the clean reconstructed Pt(100) surface and the left terraces are graphene coated. Figure 1e and f show the same area after 25 L of O_2 and 40 L of O_2, respectively. As for CO exposure, the Pt(100) reconstruction is lifted in the unprotected areas after exposure to O_2 as expected,[19] whereas the graphene coating protects the Pt(100) surface, also after doses up to 500 L of oxygen.

To investigate the coating effect toward CO and O_2 at higher partial pressures, the same type of experiments were performed with pressures up to 1.7×10^{-4} mbar. The results are presented in Figure 2. In Figure 2a, an area containing a graphene-coated part on the right-hand side and an unprotected part on the left-hand side is depicted before exposure. After exposure to 800 L and 4.4×10^{-7} mbar CO, the reconstruction is lifted in the uncoated area, whereas no detectable change is observed for the graphene-coated area (Figure 2b), exactly as presented in Figure 1c. However, after exposure to 2400 L of CO and 2.2×10^{-6} mbar, the reconstruction is lifted in the lower left part of the graphene-coated area (Figure 2c). By increasing the pressure even further, the reconstruction is lifted in the whole area after 7000 L of CO and 2×10^{-5} mbar (Figure 2d). The inset in Figure 2d shows that the basal plane of the graphene is still intact in the areas, where the reconstruction has been lifted, indicating that CO has been intercalated. A similar effect has been observed for the graphene–Pt(111) system.[16]

Figure 2e shows a similar area, where the platinum surface is partly coated by graphene, after exposure to 90 L of O_2 and 2.6×10^{-7} mbar. The result is similar to

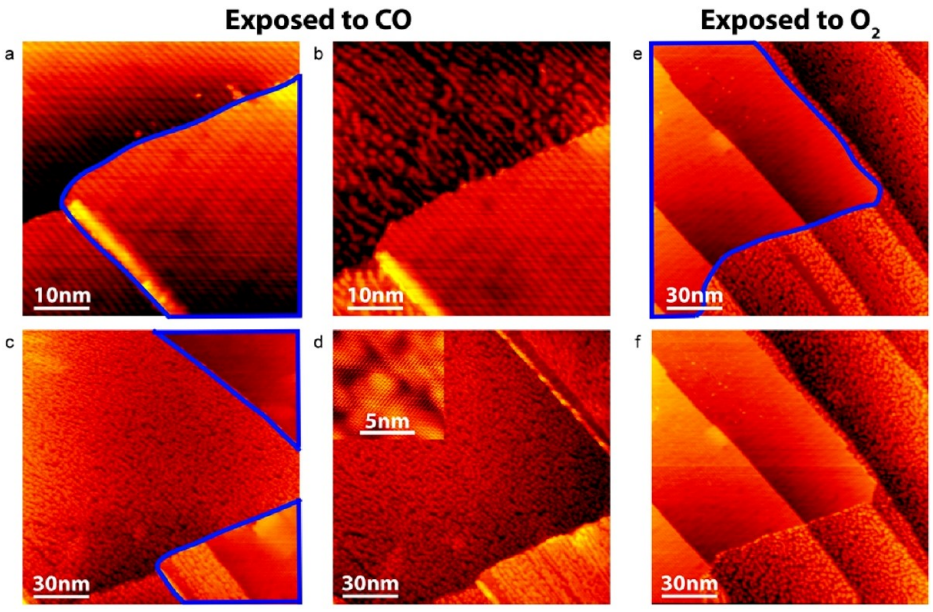

Figure 2. STM image of a Pt(100) surface partially coated by graphene. For images (a)−(d), the terrace at the right side is coated by graphene (indicated by a blue boundary), whereas the rest is uncoated. (a−d) Partially coated surface exposed to 0 and 80 L and 4.4×10^{-7} mbar, 2400 L and 2.2×10^{-6} mbar, and 7000 L and 2×10^{-5} mbar of CO, respectively. The inset in (d) shows a high-resolution depiction of the area, where the reconstruction has been lifted under the graphene. (e, f) Partially graphene-coated surface exposed to 90 L and 2.6×10^{-7} mbar and 45 000 L and 1.7×10^{-4} mbar of O_2, respectively. Imaging conditions [Vt, It]: (a) [52 mV, 0.19 nA] ; (b) [−3.4 mV, 0.14 nA] ; (c, d) [−57 mV, 0.06 nA]; (d, inset) [−4.3 mV, 0.09 nA]; (e, f) [54 mV, 0.13].

what was observed in Figure 1f, namely, the lifting of the reconstruction in the uncoated areas, whereas the coated area is undisturbed. The same finding is observed after exposing the surface to 45 000 L of O_2 and 1.7×10^{-4} mbar (Figure 2f), which demonstrates the high coating efficiency of graphene toward O_2 under these conditions.

To further investigate the efficiency of the graphene coating, a complete monolayer of graphene on Pt(100) was exposed to 2000 K hot atomic hydrogen (the D isotope was used in all experiments). In Figure 3a, the surface is depicted after having been exposed for 2 s to atomic hydrogen. A number of bright protrusions are observed. On the basis of high-resolution STM images (inset in Figure 3a) these protrusions are identified as hydrogen dimers, similar to those observed on graphite[21] and graphene on SiC.[22,23] From the orientation of the protrusions, it can be deduced that they are either para- or ortho-dimers (see inset in Figure 3a). This observation is in agreement with the theoretical findings that para- and ortho-dimers are energetically more stable than meta-dimers and monomers for single-sided hydrogenated graphene.[21,24−26] The reconstruction of the underlying Pt(100) surface is still depicted through the graphene, which indicates that the graphene coating is still effective even though it has reacted with small amounts of atomic hydrogen.

An estimate of the coverage of hydrogen atoms after 2 s of hydrogen exposure was made by counting the number of hydrogen dimers on a large-scale image. The coverage, number of hydrogen atoms per carbon atoms, was found to be *ca.* 2% after 2 s of hydrogen exposure. These experimental results are contrary to the assumption that H cannot bind on the basal plane of graphene on Pt(100) as stated by Zecho *et al.* based on TPD experiments without any local probe information.[27]

By exposing the graphene surface to a 5 s hydrogen dose (Figure 3b), the amount of bright protrusions increases; however, the protrusions are still mainly dimers and small clusters, which is also the case after a 10 s hydrogen dose (Figure 3c). In both cases the reconstruction is conserved.

Larger protrusions start to appear after ca. 20 s of hydrogen dosing (Figure 3d). After a 25 s hydrogen dose, the larger protrusions are more widespread, and it is noticed that they become elongated along the stripe direction of the graphene (Figure 3e). The surface after a 45 s dose of hydrogen is displayed in Figure 3f. At this coverage, mainly extended protrusions are depicted and the reconstruction is not visible any longer, indicating that the coating effect is compromised.

Deuterium TPD curves of the hydrogenated graphene surface are displayed in Figure 4a, including the curves with dose times corresponding to the STM pictures in Figure 3. At low coverage (below 20 s), the desorption peak temperature is increasing gradually from *ca.* 480 K to *ca.* 540 K with increasing coverage, indicating a stabilizing effect for higher coverage. After 20 s of H exposure a new peak appears, visible above 600 K as a shoulder on the main peak. After 25 s of H exposure a marked shift in the position of the low-temperature peak to *ca.* 570 K is observed and the peak

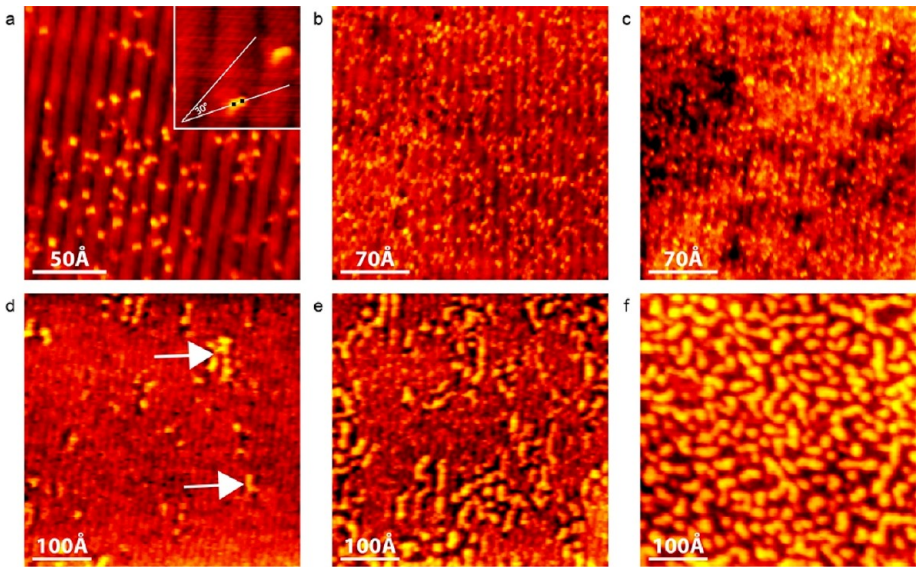

Figure 3. STM images of hydrogenated graphene on Pt(100). (a−f) Graphene exposed to atomic D for 2, 5, 10, 20, 25, and 60 s, respectively. The small bright protrusions are clusters of hydrogen atoms adsorbed to the graphene sheet. The extended bright protrusions (indicated by the two white arrows in (d)) are ascribed to the lifting of the Pt(100) reconstruction. (a, inset) High resolution of two hydrogen protrusions after 2 s of H exposure. The two white lines follow the direction of a typical hydrogen protrusion and a graphene zigzag direction, respectively. The two black squares are placed on the center axis of the protrusion separated by 2.46 Å. From the orientation, shape, and size it can be deduced that they are either ortho- or para-dimers. Imaging conditions: [Vt, It]: (a) [−234 mV, 0.27 nA], (a, inset) [−490 mV, 0.26 nA], (b) [−1445 mV, 0.43 nA], (c) [−726 mV, 0.30 nA], (d) [−972 mV, 0.27 nA], (e) [−840 mV, 0.29 nA], (f) [−525 mV, 0.31 nA].

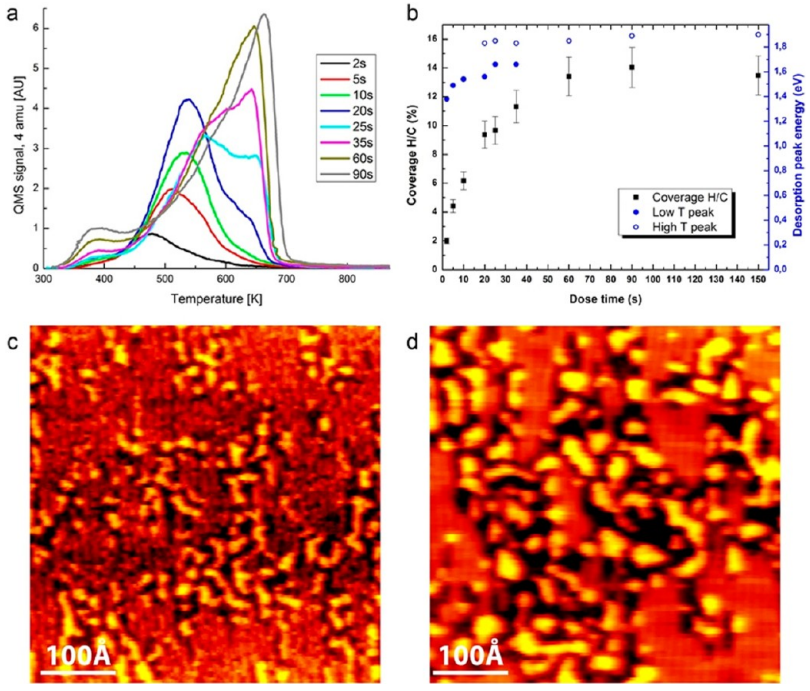

Figure 4. (a) Temperature-programmed desorption curves for hydrogen (D_2) from the fully graphene-coated Pt(100) surface. The peak shift from *ca.* 480 K to *ca.* 540 K is ascribed to desorption of hydrogen from the graphene surface, in a situation where the reconstruction of the platinum surface is not lifted, whereas the high-temperature peak is ascribed to desorption of hydrogen from the regions where the reconstruction of the platinum surface is lifted. The low-temperature peak below 400 K is related to the surroundings of the graphene surface. Ramp 1 K/s. (b) The hydrogen coverage H/C as a function of dose time (on the left *y*-axis). The desorption peak energies calculated from the TPD curves in (a) are displayed on the right *y*-axis. The low [high]-*T* peak corresponds to hydrogen desorbing from the areas without [with] the reconstruction lifted. (c) STM image of hydrogenated graphene with a mixture of regions with and without the reconstruction lifted due to the intermediate coverage. (d) STM image of the hydrogenated graphene surface after annealing to 573 K (1 K/s). Mainly the big protrusions corresponding to the regions with the reconstruction lifted are left. Imaging conditions [Vt, It]: (c) [−580 mV, 0.27 nA]; (d) [460 mV, 0.25 nA].

above 600 K is seen to increase in size, indicating a clear stabilization. For even higher coverage, the high-temperature peak becomes the main peak. For saturation coverage, the main peak is observed at 660 K.

The hydrogen coverage as a function of exposure time was estimated from the integrated TPD curves. The coverage after 2 s of hydrogen dose, obtained by counting the number of dimers on a large-scale image, was used for calibration. The coverage as a function of exposure time is displayed in Figure 4b. The saturation coverage is observed to be *ca.* 14%, and the lifting of the reconstruction starts to appear at *ca.* 9%.

From the TPD curves, the desorption energies are calculated using the Redhead method.[28] For the low-coverage regime, below 25 s of hydrogen dose, the desorption energy is observed to increase for increasing coverage. A gradual shift from 1.38 eV for the 2 s dose to 1.56 eV for the 20 s dose is observed. For the high-coverage regime, 25 s and above, desorption energies are in the range 1.8−1.9 eV. The coverage-dependent desorption energies are depicted in Figure 4b.

The dimer arrangement of the hydrogen atoms on the surface after 2 s of hydrogen exposure and the corresponding TPD peak at 480 K is very similar to hydrogen on HOPG.[21] The TPD peak at 660 K for saturation coverage is more similar to the desorption temperature for hydrogen on graphene grown on Ir(111).[29] The stabilization of hydrogen on graphene on Ir(111) is facilitated by the alternating binding of the carbon atoms in the graphene sheet to a hydrogen atom above the graphene sheet and to an iridium atom below the graphene sheet,[30] resulting in a graphane-like structure.

A similar mechanism is suggested here for graphene on Pt(100) for a coverage corresponding to more than 20 s of hydrogen exposure: in this picture the main shift in the desorption peak temperature is induced when the graphene sheet starts to bind to the reconstructed platinum substrate, whereby the reconstruction is lifted. This is in excellent agreement with the observations of extended bright protrusions, which are ascribed to extra platinum atoms below the graphene surface originating from the lifting of the reconstruction as observed in Figure 1 and found by Borg *et al.*[19] By increasing the hydrogen coverage, the lifting of the reconstruction continues, which further stabilizes the hydrogen structures, resulting in higher desorption temperatures as observed in the TPD measurements.

The relative population at energies lower than the main peak is decreasing with increasing coverage, which is in agreement with the hypothesis stated above: the high (low) desorption energy peaks correspond to the area with (without) lifted reconstruction, which increases (decreases) in prevalence for increasing coverage. The assignment of the dimer and small cluster structures to the low-temperature peak and the extended protrusions to the high-temperature peak is supported by annealing a graphene sample with an intermediate coverage to 573 K. Mainly the extended protrusions are left after annealing, whereas the dimer structures are desorbed (see Figure 4c and d). By annealing the sample above 700 K the clean graphene on the reconstructed platinum surface was re-formed.

The suggestion that a lifting of the reconstruction becomes favorable for a H coverage about 9% is corroborated by DFT calculations carried out within the generalized gradient approximation (GGA). The hex-reconstructed Pt(100) surface was described by the commonly used approximate unit cell consisting of a (1×5) Pt(100) slab with a quasi-hexagonal layer on top compressed by 4% in one direction, but uncompressed in the other direction.[31] From previous studies[5] it is known that the graphene layer can have different rotations with respect to the reconstructed Pt(100) surface. In this study, however, only the two most commonly observed rotations with either the graphene armchair (rotation 1) or the graphene zigzag (rotation 2) direction aligned with the close-packed direction of the hex-reconstructed layer were taken into account.

The results for rotation 1 are illustrated in Figure 5. The graph shows the energy difference per surface area as a function of the H/C coverage between the final (F) Pt/graphene/H configurations where the reconstruction is lifted and the initial (I) configurations where the Pt(100) surface reconstruction is preserved underneath the graphene. From the STM images in Figure 3 it is possible to determine only the configuration of the H atoms in the initial configuration (before lifting the reconstruction) for the lowest coverage (see inset in Figure 3a), whereas for higher coverage a high-resolution image of a separate H cluster cannot be obtained. Therefore two limiting cases for the arrangement of the H atoms in the initial configuration were investigated: In the upper right structure in Figure 5 ($I^{cluster}_{high\theta}$), all H atoms were arranged in a large cluster, stabilized by bonding between the graphene sheet and the underlying hex-reconstructed Pt layer. The configuration shown corresponds to the most stable structure found. When testing different configurations of the H atoms, it was evident that the most stable structures include hydrogenated carbon atoms positioned in hollow sites with respect to the underlying Pt lattice, whereas for carbon atoms in top sites it is more favorable to bend downward and bond to the underlying Pt atom (see side view). The obtained structure is similar to previously proposed graphane-like clusters formed on graphene on transition metal substrates;[30] however, due to the specific rotation of the graphene sheet, a true graphane-like structure where every other carbon atom binds to a H atom above and every other to a Pt atom below cannot be realized. Instead, the structure is comparable to the proposed boat-like configuration of graphane.[32] In the

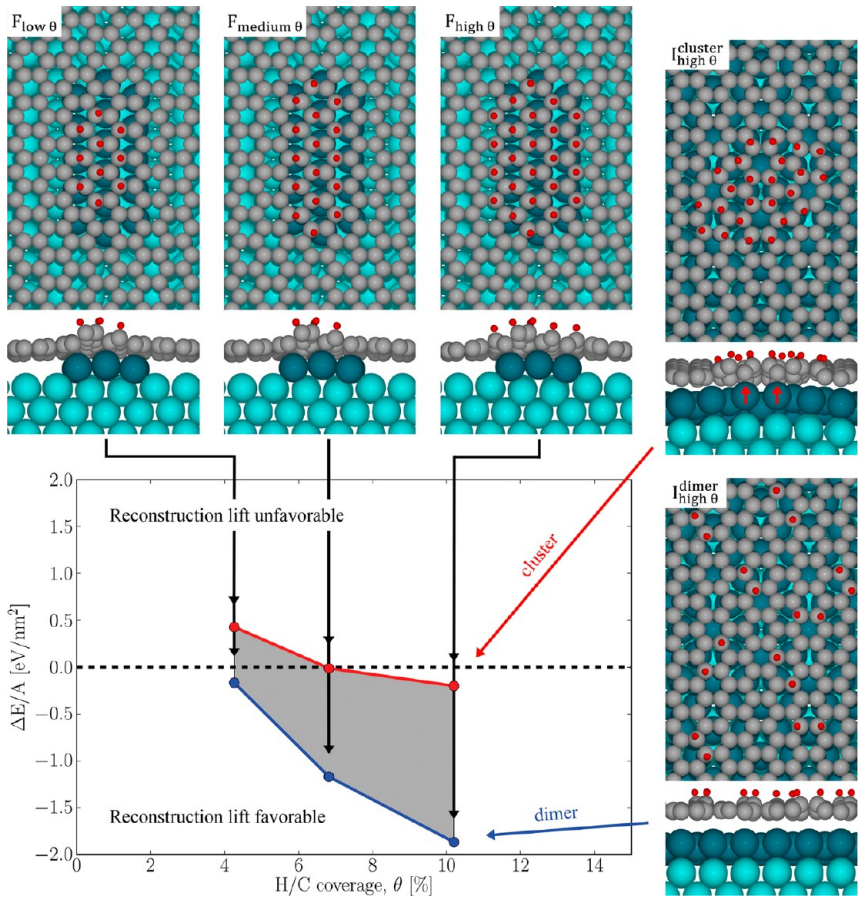

Figure 5. Graph of the energy difference per surface area as a function of the H/C coverage, θ, between the final (F) Pt/graphene/H configurations, where the reconstruction is lifted and the extra Pt atoms arranged in an island (top left structures), and the initial (I) configurations on rotation 1, where the Pt(100) surface reconstruction is preserved underneath the graphene (right structures). Top views and side views cut through the middle of a cluster. Pt atoms in (100) [(111)] layers are colored light [dark] blue, C atoms are gray, and H atoms are red. The energy difference, ΔE, is defined as $\Delta E = E(F_\theta) - E(I^i_\theta) + \Delta E_\mu$, where θ is the H/C coverage, i refers to either cluster or dimer initial configurations, and ΔE_μ adjusts for the different number of atoms in the structures to be compared and includes the chemical potentials of a graphene layer on an unreconstructed and on a reconstructed Pt(100) surface with no H attached (see Supporting Information for further details). The filled gray area in the graph illustrates the uncertainty in determining the initial configuration from the STM images in Figure 3. The two limiting cases are dimer (blue dots) and cluster (red dots) initial configurations.

side view it is seen how the interaction with the substrate lifts Pt atoms somewhat out of the hex-reconstructed layer (red arrows), which is expected to facilitate the lifting of the reconstruction. The lower right structure in Figure 5 (I^{dimer}_{high}) corresponds to dimers of adsorbed H atoms with no substrate interaction (see side view), which in the STM images was identified as the dominant configuration at low H coverage. The experimental uncertainty in determining the initial configurations, and thereby the uncertainty in the calculated energy difference when lifting the reconstruction, is illustrated with the filled gray area in the graph in Figure 5.

For the final configurations (after lifting the reconstruction) the extra Pt atoms were arranged in an island and the H atoms were placed on the graphene covering this island (top left structures in Figure 5). The structures shown were found to be energetically most stable from a systematic search, varying both the size and shape of the Pt islands and the configuration of the H atoms. An elongated shape of the Pt islands was found to be most favorable, in good agreement with the structures observed in STM after lifting the reconstruction (see Figure 3e and f). The obtained structures are almost graphane-like with an alternating bonding of the carbon atoms to H atoms above and to Pt atoms in the island below. However, due to the mismatch between the graphene and Pt lattice constants, it is favorable to introduce an extra row of H atoms along the central row of Pt atoms in the island. Such details in the configuration of the H atoms cannot be examined in the STM images in Figure 3.

In evaluating the energetics of lifting the reconstruction, three different values of H coverage were investigated, and, for each, the energy difference was evaluated with respect to both the dimer and cluster type of initial configuration. Overall, the results indicate that if the initial configuration is dimers of adsorbed H atoms, the reconstruction lifting is favorable at all values of H

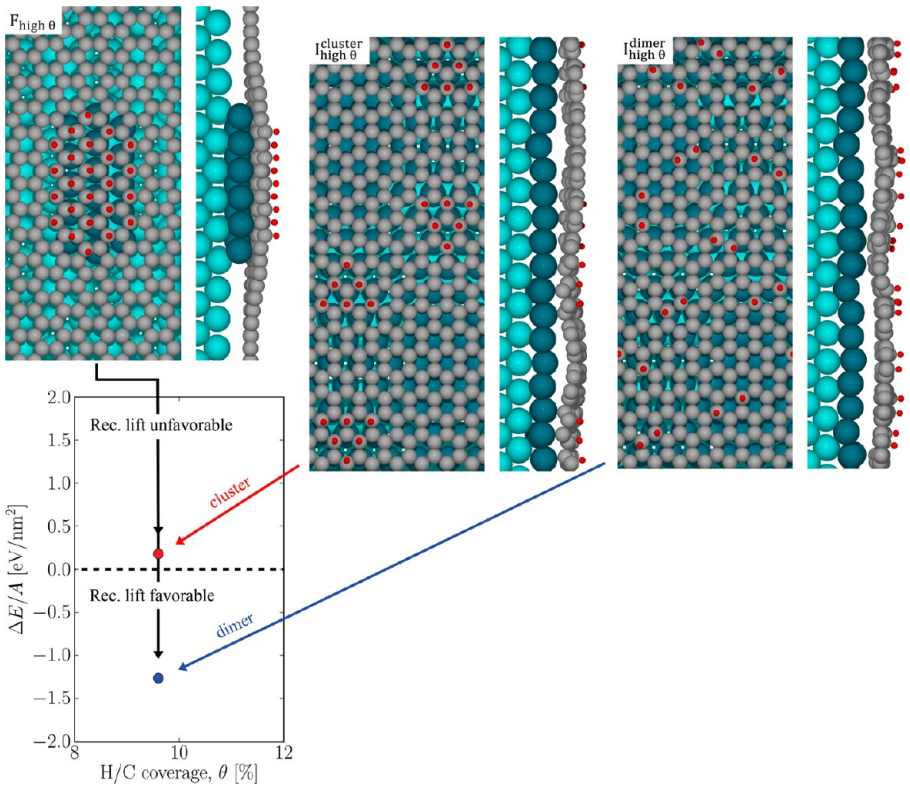

Figure 6. Graph of the energy difference per surface area between the final (F) Pt/graphene/H configuration, where the reconstruction is lifted (upper left structure), and the dimer and cluster initial (I) configurations on rotation 2, where the Pt(100) surface reconstruction is preserved underneath the graphene (2 lower right structures), for high (9.6%) H/C coverage. Top views and side views cut through the middle of a cluster. Pt atoms in (100) [(111)] layers are colored light [dark] blue, C atoms are gray, and H atoms are red. See caption to Figure 5 for a definition of ΔE.

coverage investigated (4−10%) by between 0.2 and 1.9 eV/nm^2, whereas if the initial configuration is large clusters stabilized by substrate interaction, the lifting of the reconstruction becomes favorable for an H coverage around 7%, reaching a value of 0.2 eV/nm^2 at 10% coverage. This is in excellent agreement with the experimental results.

The results for rotation 2 are given in Figure 6. For this rotation only the highest coverage was investigated. The results indicate that if the initial configuration is dimers of adsorbed H atoms, the reconstruction lifting is favorable by 1.3 eV/nm^2, whereas if the initial configuration is large clusters stabilized by substrate interaction, the reconstruction lifting is unfavorable by 0.2 eV/nm^2. The main difference from rotation 1 is that when the graphene zigzag direction is aligned with the Pt close-packed direction, true graphane-like clusters can be formed in the initial ($I^{cluster}$) configuration (before lifting the reconstruction). These clusters are more stable than the large clusters that can be formed on rotation 1, whereby the lifting of the reconstruction becomes unfavorable. A minor difference from rotation 1 is that for the dimer initial configuration it can be favorable for the carbon atoms next to a H dimer to bend downward and bond to the underlying Pt atom (see side view). This depends on the exact position of the carbon atoms with respect to the hex-reconstructed Pt(100) layer beneath.

Overall, the experimental data suggest that the lifting of the reconstruction occurs over the entire surface, whereas the computational results suggest that there could be a difference between differently rotated domains. However, the computational results will be in agreement with the experimental results if it is assumed that the initial configuration on both domains corresponds to dimers or a combination of dimers and larger clusters, as suggested by the low-coverage STM images. The exclusive arrangement of all H atoms into large graphane-like clusters before the lifting of the reconstruction seems unrealistic, since such structures require a registry between the graphene and the hex-reconstructed Pt(100) surface with carbon atoms directly on top of Pt atoms (see cluster initial configurations for rotation 1 in Figure 5 and for rotation 2 in Figure 6). After the lifting of the reconstruction, the extra Pt atoms on the surface have more degrees of freedom to assemble into clusters on areas of the Pt(100) surface, where the registry with graphene facilitates the formation of graphane-like structures.

Calculated barriers for H_2 desorption also corroborate that the reconstruction is lifted at high coverage. For the final configuration at high coverage (F_{high} in Figure 5), barriers for H_2 desorption were calculated for different sets of H atoms in the cluster. It was found that the outer rows of H atoms desorb with barriers around

1.6 eV, whereas the H atoms toward the center of the cluster desorb with a barrier around 2.1 eV. From the TPD curves the barriers for H_2 desorption at the highest coverage were found to be within the range 1.8−1.9 eV (see Figure 4a). There is a good qualitative agreement between calculations and experimental results, since the peaks at high coverage in the TPD spectrum (see Figure 4a) are observed to have a long tail toward lower binding energies, which could correspond to looser bound H at the edges of the clusters.

CONCLUSION

In summary, we have shown that graphene can work effectively as a corrosion-inhibiting coating on metal surfaces against O_2 exposure at partial pressures as high as 10^{-4} mbar, whereas the coating effect was observed to break down for partial pressures of CO above *ca.* 1×10^{-6} mbar, due to intercalation of CO. In the extreme case of 2000 K hot atomic hydrogen exposure, the graphene coating was observed to react with the hydrogen atoms, and at a coverage above 8−10%, the hydrogen adsorbates were seen to induce a lifting of the reconstruction.

While for the CO-induced lifting of the reconstruction, the molecules were observed to intercalate under the graphene and get in direct contact with the metal surface, the hydrogen-induced lifting of the reconstruction involved no direct contact between the metal surface and the hydrogen atoms. Rather, DFT calculations suggested a graphene-mediated mechanism, where carbon atoms in the graphene sheet bend downward and bond to the platinum atoms below. Even after extensive exposure to 2000 K hot atomic hydrogen (*i.e.*, Figure 3f), the hex-reconstruction of the metal surface and the graphene coating could be completely recovered by a simple thermal anneal to 700 K. This demonstrates that the graphene basal plane stays intact even under the harsh conditions of 2000 K atomic hydrogen exposure and prevents direct interactions between the substrate and the hydrogen atoms.

METHODS

The Pt(100) surface was cleaned by standard sputter/anneal (900 °C) cycles. At the end of the last anneal period, the surface was exposed to 4×10^{-7} Torr of ethylene for 40 min at 700 °C. Thereafter the ethylene gas was pumped out, and the sample was annealed at 800 °C for 5 min. This procedure results in a complete monolayer of graphene. To prepare a surface with a partial graphene coating, the same procedure was followed; however, the surface was exposed to only 2×10^{-7} Torr of ethylene for 10 min and still postannealed at 800 °C for 5 min.

The experimental results were obtained at room temperature in two ultrahigh-vacuum chambers with a base pressure below 2×10^{-10} Torr. The chambers were equipped with a so-called Aarhus STM,[33] a quadrupole mass spectrometer for TPD spectroscopy, a thermal hydrogen atom beam source,[34] and various gas inlets. All STM pictures and TPD curves of the hydrogenated graphene were obtained from the same graphene sample; that is, the graphene was annealed between each experiment to desorb the hydrogen, however, not regrown.

The calculations regarding the energetics of lifting the reconstruction were performed with the SIESTA code[35,36] for reasons of computational efficiency, since the unit cells involved several hundreds of atoms. The PBE functional[37] was used for exchange and correlation. The numerical atomic orbital basis set quality was double-ζ plus polarization orbitals, and the range of the orbitals was defined through an orbital energy shift of 0.01 Ry. A mesh cutoff value of 150 Ry was used for the plane waves in the real space grid. The effects of the core electrons were described using norm-conserving pseudopotentials of the improved Trouiller-Martins type.[38] For the initial configurations (before lifting the reconstruction) on rotation 1 the slabs were modeled by four (6×10) Pt(100) layers followed by a (6×12) quasi-hexagonal Pt layer and a (4 armchair lattice constants × 11 zigzag lattice constants) graphene layer, whereas on rotation 2 the slabs were modeled by four (6×15) Pt(100) layers followed by a (6×18) quasi-hexagonal Pt layer and a (7 zigzag lattice constants × 10 armchair lattice constants) graphene layer. For the final configuration (after lifting the reconstruction) on rotation 1, the slabs were modeled by five (6×10) Pt(100) layers followed by an island of 16 Pt atoms and a (4 armchair lattice constants × 11 zigzag lattice constants) graphene layer, whereas on rotation 2 the slabs were modeled by five (6×12) Pt(100) layers followed by an island of 16 Pt atoms and a (4 armchair lattice constants × 14 zigzag lattice constants) graphene layer. The optimized graphene lattice constant of 2.490 Å was used, and the Pt lattice constant was adapted accordingly. The mismatch with the optimized Pt lattice constant is within the range [−3.87%; 1.96%], a reasonable approximation. A (2,1) k-point grid was used for all cells. 3D periodic boundary conditions were employed, and a vacuum layer of 15 Å in the direction normal to the surface separated adjacent slabs.

The calculations regarding the barriers for H_2 desorption were performed with the GPAW code,[39] since much smaller unit cells were sufficient for these calculations. The PBE functional was used for exchange and correlation. Zero-point vibrational energies were not taken into account. The slabs were modeled with two (6×7) Pt(100) layers followed by an island of 16 Pt atoms and a (4 armchair lattice constants × 8 zigzag lattice constants) graphene layer. 2D periodic boundary conditions were employed parallel to the slab, and a vacuum layer of 7.5 Å separated the slab from the edges of the cell. Only the Γ point was used for Brillouin zone sampling. The grid spacing was 0.20 Å. The graphene lattice constant was fixed to its optimized value of 2.467 Å, and the Pt lattice constants were adapted accordingly. The mismatch with the optimized Pt lattice constant is 2.47% and 1.42% along the *x*- and *y*-axis, respectively.

For all calculations the bottom Pt(100) layer was kept fixed, and the remaining atoms were relaxed until the max force on every atom was below 0.05 eV/Å.

Conflict of Interest: The authors declare no competing financial interest.

Acknowledgment. We acknowledge financial support from the European Research Council under ERC starting grant "HPAH", No. 208344, from the Danish Council for Independent Research, Natural Sciences, from the Danish Council for Independent Research, Technology and Production Sciences, and from the Lundbeck Foundation.

Supporting Information Available: Details on calculating the energy difference when lifting the reconstruction. This material is available free of charge *via* the Internet at http://pubs.acs.org.

REFERENCES AND NOTES

1. Novoselov, K. S.; Geim, A. K.; Morozov, S. V.; Jiang, D.; Zhang, Y.; Dubonos, S. V.; Grigorieva, I. V.; Firsov, A. A. Electric Field Effect in Atomically Thin Carbon Films. *Science* **2004**, *306*, 666–669.

2. Geim, A. K.; Novoselov, K. S. The Rise of Graphene. *Nat. Mater.* **2007**, *6*, 183–191.
3. Coraux, J.; N'Diaye, A. T.; Busse, C.; Michely, T. Structural Coherency of Graphene on Ir(111). *Nano Lett.* **2008**, *8*, 565–570.
4. Wintterlin, J.; Bocquet, M. L. Graphene on Metal Surfaces. *Surf. Sci.* **2009**, *603*, 1841–1852.
5. Nilsson, L.; Andersen, M.; Bjerre, J.; Balog, R.; Hammer, B.; Hornekær, L.; Stensgaard, I. Preservation of the Pt(100) Surface Reconstruction after Growth of a Continuous Layer of Graphene. *Surf. Sci.* **2012**, *606*, 464–469.
6. Sutter, P.; Sadowski, J. T.; Sutter, E. A. Chemistry under Cover: Tuning Metal-Graphene Interaction by Reactive Intercalation. *J. Am. Chem. Soc.* **2010**, *132*, 8175–8179.
7. Borca, B.; Calleja, F.; Hinarejos, J. J.; de Parga, A. L. V.; Miranda, R. Reactivity of Periodically Rippled Graphene Grown on Ru(0001). *J. Phys. Condens. Mater.* **2009**, *21*, 134002.
8. Dedkov, Y. S.; Fonin, M.; Laubschat, C. A Possible Source of Spin-Polarized Electrons: The Inert Graphene/Ni(111) System. *Appl. Phys. Lett.* **2008**, *92*, 052506.
9. Chen, S.; Brown, L.; Levendorf, M.; Cai, W.; Ju, S.-Y.; Edgeworth, J.; Li, X.; Magnuson, C. W.; Velamakanni, A.; Piner, R. D.; *et al.* Oxidation Resistance of Graphene-Coated Cu and Cu/Ni Alloy. *ACS Nano* **2011**, *5*, 1321–1327.
10. Topsakal, M.; Sahin, H.; Ciraci, S. Graphene Coatings: An Efficient Protection from Oxidation. *Phys. Rev. B* **2012**, *85*, 155445.
11. Kirkland, N. T.; Schiller, T.; Medhekar, N.; Birbilis, N. Exploring Graphene as a Corrosion Protection Barrier. *Corros. Sci.* **2012**, *56*, 1–4.
12. Prasai, D.; Tuberquia, J. C.; Harl, R. R.; Jennings, G. K.; Bolotin, K. I. Graphene: Corrosion-Inhibiting Coating. *ACS Nano* **2012**, *6*, 1102–1108.
13. Cho, J.; Gao, L.; Tian, J.; Cao, H.; Wu, W.; Yu, Q.; Yitamben, E. N.; Fisher, B.; Guest, J. R.; Chen, Y. P.; *et al.* Atomic-Scale Investigation of Graphene Grown on Cu Foil and the Effects of Thermal Annealing. *ACS Nano* **2011**, *5*, 3607–3613.
14. Vinogradov, N. A.; Schulte, K.; Ng, M. L.; Mikkelsen, A.; Lundgren, E.; Mårtensson, N.; Preobrajenski, A. B. Impact of Atomic Oxygen on the Structure of Graphene Formed on Ir(111) and Pt(111). *J. Phys. Chem. C* **2011**, *115*, 9568–9577.
15. Gadipelli, S.; Calizo, I.; Ford, J.; Cheng, G.; Walker, A. R. H.; Yildirim, T. A Highly Practical Route for Large-Area, Single Layer Graphene from Liquid Carbon Sources Such as Benzene and Methanol. *J. Mater. Chem.* **2011**, *21*, 16057–16065.
16. Mu, R.; Fu, Q.; Jin, L.; Yu, L.; Fang, G.; Tan, D.; Bao, X. Visualizing Chemical Reactions Confined under Graphene. *Angew. Chem., Int. Ed.* **2012**, *51*, 4856–4859.
17. May, J. W. Platinum Surface Leed Rings. *Surf. Sci.* **1969**, *17*, 267–270.
18. Helveg, S.; Lopez-Cartes, C.; Sehested, J.; Hansen, P. L.; Clausen, B. S.; Rostrup-Nielsen, J. R.; Abild-Pedersen, F.; Norskov, J. K. Atomic-Scale Imaging of Carbon Nanofibre Growth. *Nature* **2004**, *427*, 426–429.
19. Borg, A.; Hilmen, A. M.; Bergene, E. STM Studies of Clean, CO-Exposed and O_2-Exposed Pt(100)-Hex-R0.7-Degrees. *Surf. Sci.* **1994**, *306*, 10–20.
20. Hu, X.; Lin, Z. Hydrogen-Adsorption-Induced Phase Transitions on Pt(100)-Hex and the Surface Structure of Pt(100)-(1×1)H. *Phys. Rev. B: Condens. Matter* **1995**, *52*, 11467.
21. Hornekaer, L.; Sljivancanin, Z.; Xu, W.; Otero, R.; Rauls, E.; Stensgaard, I.; Laegsgaard, E.; Hammer, B.; Besenbacher, F. Metastable Structures and Recombination Pathways for Atomic Hydrogen on the Graphite (0001) Surface. *Phys. Rev. Lett.* **2006**, *96*, 156104.
22. Balog, R.; Jorgensen, B.; Wells, J.; Laegsgaard, E.; Hofmann, P.; Besenbacher, F.; Hornekaer, L. Atomic Hydrogen Adsorbate Structures on Graphene. *J. Am. Chem. Soc.* **2009**, *131*, 8744–8745.
23. Guisinger, N. P.; Rutter, G. M.; Crain, J. N.; First, P. N.; Stroscio, J. A. Exposure of Epitaxial Graphene on SiC(0001) to Atomic Hydrogen. *Nano Lett.* **2009**, *9*, 1462–1466.
24. Sljivancanin, Z.; Rauls, E.; Hornekaer, L.; Xu, W.; Besenbacher, F.; Hammer, B. Extended Atomic Hydrogen Dimer Configurations on the Graphite(0001) Surface. *J. Chem. Phys.* **2009**, *131*, 084706.
25. Casolo, S.; Lovvik, O. M.; Martinazzo, R.; Tantardini, G. F. Understanding Adsorption of Hydrogen Atoms on Graphene. *J. Chem. Phys.* **2009**, *130*, 054704.
26. Ferro, Y.; Teillet-Billy, D.; Rougeau, N.; Sidis, V.; Morisset, S.; Allouche, A. Stability and Magnetism of Hydrogen Dimers on Graphene. *Phys. Rev. B* **2008**, *78*, 085417.
27. Zecho, T.; Horn, A.; Biener, J.; Kuppers, J. Hydrogen Atom Reactions with Monolayer Graphite Edges on Pt(100) Surfaces: Hydrogenation and H Abstraction. *Surf. Sci.* **1998**, *397*, 108–115.
28. Redhead, P. A. Thermal Desorption of Gases. *Vacuum* **1962**, *12*, 203–211.
29. Jorgensen, B.; Thrower, J.; Baouche, S.; Balog, R.; Nilsson, L.; Friis, E. E.; Baurichter, A.; Zecho, T.; Besenbacher, F.; Luntz, A., *et al.* Substrate Enhanced Stability of Hydrogen Adsorption Complexes on Graphene on Ir(111). Unpublished.
30. Balog, R.; Jorgensen, B.; Nilsson, L.; Andersen, M.; Rienks, E.; Bianchi, M.; Fanetti, M.; Laegsgaard, E.; Baraldi, A.; Lizzit, S.; *et al.* Bandgap Opening in Graphene Induced by Patterned Hydrogen Adsorption. *Nat. Mater.* **2010**, *9*, 315–319.
31. Havu, P.; Blum, V.; Havu, V.; Rinke, P.; Scheffler, M. Large-Scale Surface Reconstruction Energetics of Pt(100) and Au(100) by All-Electron Density Functional Theory. *Phys. Rev. B* **2010**, *82*, 161418.
32. Sofo, J. O.; Chaudhari, A. S.; Barber, G. D. raphane: A Two-Dimensional Hydrocarbon. *Phys. Rev. B* **2007**, *75*, 153401.
33. Laegsgaard, E.; Besenbacher, F.; Mortensen, K.; Stensgaard, I.; Fully, A Automated, Thimble-Size Scanning Tunnelling Microscope. *J. Microsc. (Oxford, U.K.)* **1988**, *152*, 663–669.
34. Tschersich, K. G. Intensity of a Source of Atomic Hydrogen Based on a Hot Capillary. *J. Appl. Phys.* **2000**, *87*, 2565–2573.
35. Artacho, E.; Anglada, E.; Dieguez, O.; Gale, J. D.; Garcia, A.; Junquera, J.; Martin, R. M.; Ordejon, P.; Pruneda, J. M.; Sanchez-Portal, D.; *et al.* The Siesta Method; Developments and Applicability. *J. Phys. Condens. Mater* **2008**, *20*, 064208.
36. Soler, J. M.; Artacho, E.; Gale, J. D.; Garcia, A.; Junquera, J.; Ordejon, P.; Sanchez-Portal, D. The Siesta Method for Ab Initio Order-N Materials Simulation. *J. Phys. Condens. Mater* **2002**, *14*, 2745–2779.
37. Perdew, J. P.; Burke, K.; Ernzerhof, M. Generalized Gradient Approximation Made Simple. *Phys. Rev. Lett.* **1996**, *77*, 3865–3868.
38. Troullier, N.; Martins, J. L. Efficient Pseudopotentials for Plane-Wave Calculations. *Phys. Rev. B* **1991**, *43*, 1993–2006.
39. Enkovaara, J.; Rostgaard, C.; Mortensen, J. J.; Chen, J.; Dulak, M.; Ferrighi, L.; Gavnholt, J.; Glinsvad, C.; Haikola, V.; Hansen, H. A.; *et al.* Electronic Structure Calculations with GPAW: A Real-Space Implementation of the Projector Augmented-Wave Method. *J. Phys. Condens. Mater* **2010**, *22*, 253202.